DOI: 10.35840/2631-5092/4549

VIBGYOR ePress

International Journal of
Optics and Photonic Engineering

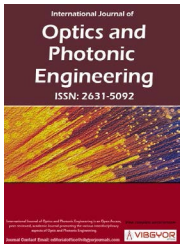

ISSN: 2631-5092

Highly Integrated Polarization Beam Splitter Based on Sin-LNOI Rib Waveguide

Wei Ji*, Fengyu Liu, Qian Wu and Rui Yin*

School of Information Science and Engineering, Shandong University, Qingdao, Shandong, China

Abstract

We propose a multimode interference (MMI)-based polarization beam splitter (PBS) in X-cut lithium niobate on insulator (LNOI). The device utilizes the high birefringence of Lithium Niobate (LiNbO3, LN) and the integration of silicon nitride (SiN) to form a PBS ridge waveguide structure. By using three dimensional finite difference time domain (3D-FDTD) method, simulation results show that the length of MMI is 190.3 μm, extinction ratio is more than 15 dB, and fabrication tolerance of waveguide width variation is about 200 nm. It not only meets the good polarization separation characteristics of TE and TM, but also has excellent process realizable characteristics.

Keywords

Polarization beam splitter, Lithium niobate on insulator, Silicon nitride, Multimode interference

Introduction

With the increasing demand for interconnection of optical communication networks, a growing interest in optical devices to deal with polarization is noticed. As an important part of optical devices, polarization beam splitter (PBS) can separate the polarization states of TE and TM in optical signals. As a novel material system in integrated photonics, lithium niobate on insulator (LNOI) offers excellent electro-optic, acousto-optic and nonlinear optical properties [1]. At the same time, for LNOI, a favorable high refractive index contrast structure is a thin single crystal LN film on a SiO_2 layer deposited on a LN-substrate with a refractive index difference of 0.7 [2-4]. In order to further obtain efficient and compact PBS, LNOI platform has attracted more and more attention in recent years. Many different structures of waveguide PBS based on integrated photonic platform have been reported, such as directional coupler (DC) [5-12], Mach-Zehnder interferometer (MZI) [13-15], multimode interference (MMI) [16-18], and photonic crystal (PhC) structures [19-21]. MMI is the one of commonly used structure to realize compact PBS, due to its simple principle and structure.

At present, LNOI based on smart slicing mode can be commercially produced [1-4], but LN thin films are difficult to be etched in the process, which usually results in large waveguide etching loss. Therefore, for LNOI, we need to combine LN thin films with semiconductor films which are more easy to be etched by means of hybrid integration. As a multi-purpose semiconductor material, SiN has good chemical composition and optical properties.

***Corresponding author:** *Wei Ji, School of Information Science and Engineering, Shandong University, Qingdao, Shandong, 266237, China; Rui Yin, School of Information Science and Engineering, Shandong University, Qingdao, Shandong, 266237, China*

Accepted: September 09, 2022; **Published:** September 11, 2022

Citation: Ji W, Liu F, Wu Q, Yin R, (2022) Highly Integrated Polarization Beam Splitter Based on Sin-LNOI Rib Waveguide. Int J Opt Photonic Eng 7:049

In the thin film waveguide layer based on SiN, the LNOI ridge waveguide structure is formed by etching SiN film and LN film together, which can solve the difficult problem of LN thin film etching [22-24].

In this paper, we propose a multimode interference (MMI)-based PBS, which is designed and implemented based on the hybrid integrated LNOI material of the thin film waveguide layer. The polarization separation of TE and TM is carried out by using the birefringence effect of the LN crystal. At the same time, because the refractive index of the SiN waveguide is lower than that of the LN waveguide, the light field can be better limited in the LN film. As a result, the waveguide loss caused by etching process is further reduced. The structure design of the MMI also greatly improves the fabrication process tolerance of the device. Through theoretical analysis and FDTD simulation, the geometric parameters of PBS are optimized to ensure the small size and high extinction ratio of the device.

Principle and Design

The principle of the MMI-based PBS

We propose the MMI-based PBS in X-cut LNOI. For the MMI, when the input contains two polarization signals of TE and TM, the propagation constants of the excited super modes are different because the excited super modes have odd modes and even modes, β_e^{TE}, β_o^{TE}, β_e^{TM} and β_o^{TM}, respectively. When there is a phase difference of π or an integer multiple of π between two super modes, the light is fully coupled into the adjacent waveguide, and for the MMI, the light is coupled from one side to the other in the wide waveguide. As long as the optical transmission distance is an integral multiple of the single coupling length, this transfer occurs periodically [25].

Due to the difference of polarization propagation constant between TE and TM, the coupling length L_C^{TE} and L_C^{TM} are given by

$$L_C^{TE} = \frac{\pi}{\beta_e^{TE} - \beta_o^{TE}} \quad (1)$$

$$L_C^{TM} = \frac{\pi}{\beta_e^{TE} - \beta_o^{TM}} \quad (2)$$

respectively. So the overall length of the coupling region L_{cr} could satisfy $L_{cr} = nL_C^{TE} = (n+1)L_C^{TM}$, for n = 1,2,3….When n is even as shown in Figure 1a, TE will output from the through port, and TM will output from the cross port, and when n is odd as shown in Figure 1b, TE will output from the cross port, and TM will output from the through port.

Parameter optimization and design

In the design of SiN-$LiNbO_3$ composite waveguide

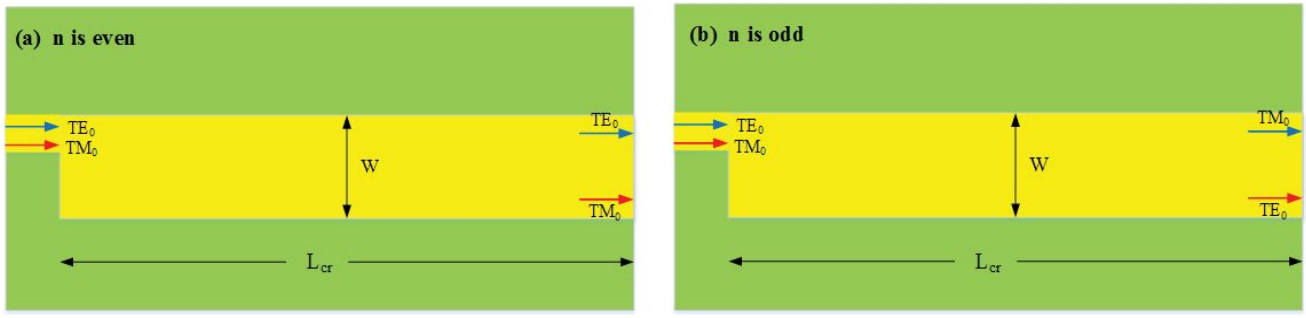

Figure 1: The schematic of the MMI-based PBS.

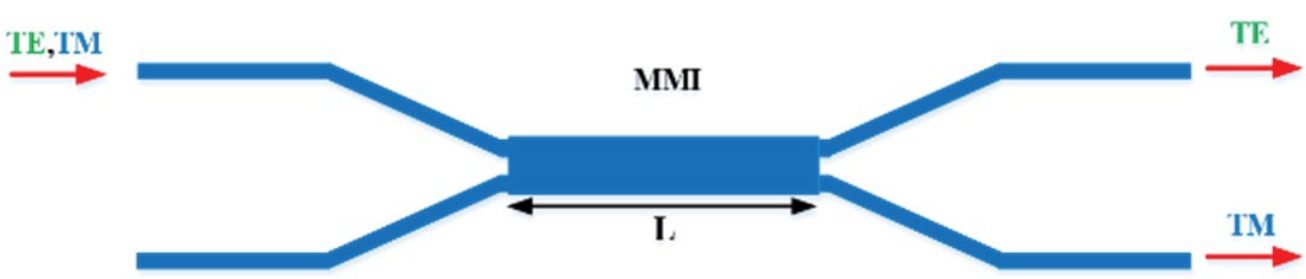

Figure 2: The top view of the proposed MMI-based PBS.

structure using PBS based on this principle, the difficulty of device process realization is reduced, and a larger waveguide fabrication tolerance is obtained at the same time. Due to the anisotropy of the LNOI platform, the refractive index of the two polarization states of TE and TM is quite different, so the two polarization states of TE and TM can be separated in a short coupling region, thus reducing the size of the whole device and improving the overall integration of the PBS in the LNOI.

Figure 2 shows the top view of the proposed MMI -based PBS, and Figure 3 shows the 3D view of the multimode interference region X-cut LNOI waveguide. In this design, the central wavelength of PBS is λ = 1550 nm. For SiN-$LiNbO_3$ composite waveguides, the refractive index of SiN is $n_{SiN} = 2.0$, the refractive index of LN is $n_e = 2.1381$, $n_o = 2.2112$, and the refractive index of SiO_2 is $n_{SiO2} = 1.4448$.

For the MMI, in rib waveguide design, the width of SiN waveguide layer is very sensitive to the limitation of single-mode and dual-mode transmission conditions. Before the light enters the MMI, the width of the SiN waveguide W_{SiN} and the thickness of the LN waveguide layer h_{LN} need to be limited to ensure the single-mode transmission condition of the rib waveguide. When the TE and TM mode optical signal enter the MMI, the width of the SiN waveguide W_{SiN} in the multimode interference region is designed to ensure that the dual-polarization optical signal can maintain dual-mode transmission in the MMI. In TE mode, Figure 4a and Figure 4b respectively simulate two different cross sections of the ridge waveguide in single-mode transmission and dual-mode transmission.

As a single-mode waveguide, we use the LN thin film layer $h_{LN} = 0.2\ \mu m$, the width of the SiN waveguide $W_{SiN} = 0.6\ \mu m$ and the thickness of the SiN waveguide $h_{SiN} = 0.4\ \mu m$ as example. Figure 4a can be seen that most of the light field can be well confined to the LN thin film, which reduces the waveguide loss caused by etching SiN thin films and reduces the insertion loss of PBS. Simultaneously, it also reduces the difficulty of fabrication in PBS process based on LNOI. Then we use FDTD simulation

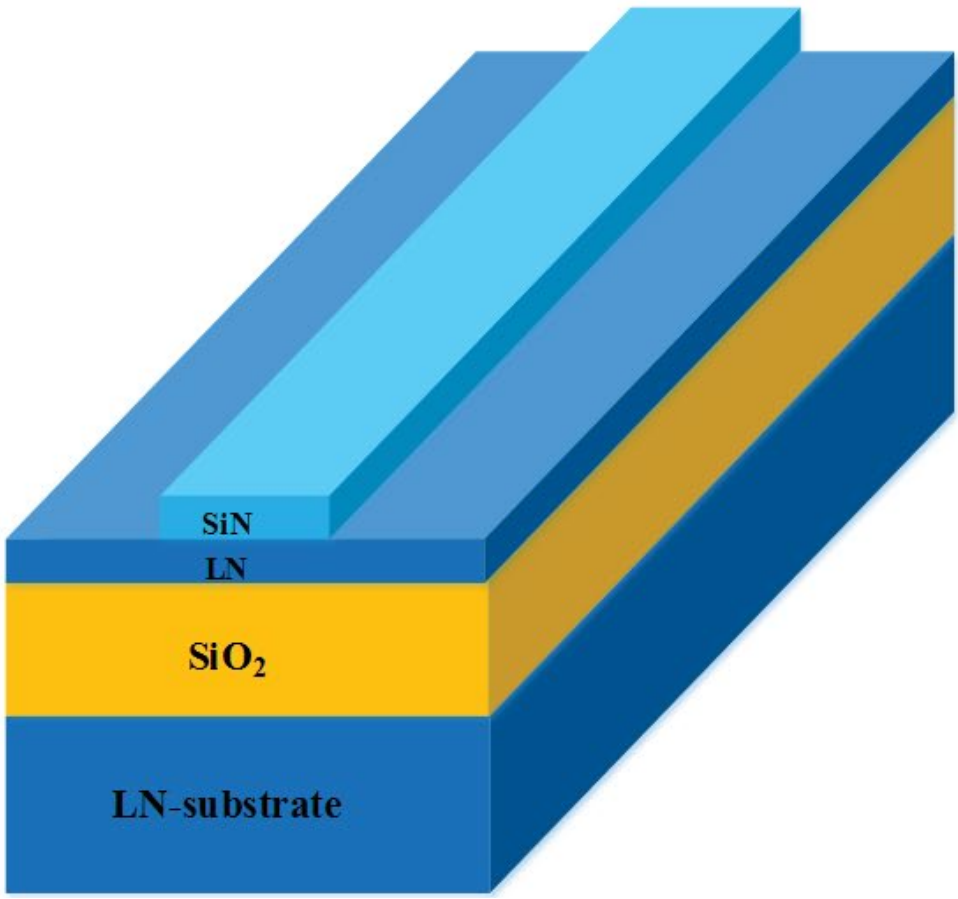

Figure 3: The 3D view for the SiN-LNOI rib waveguide.

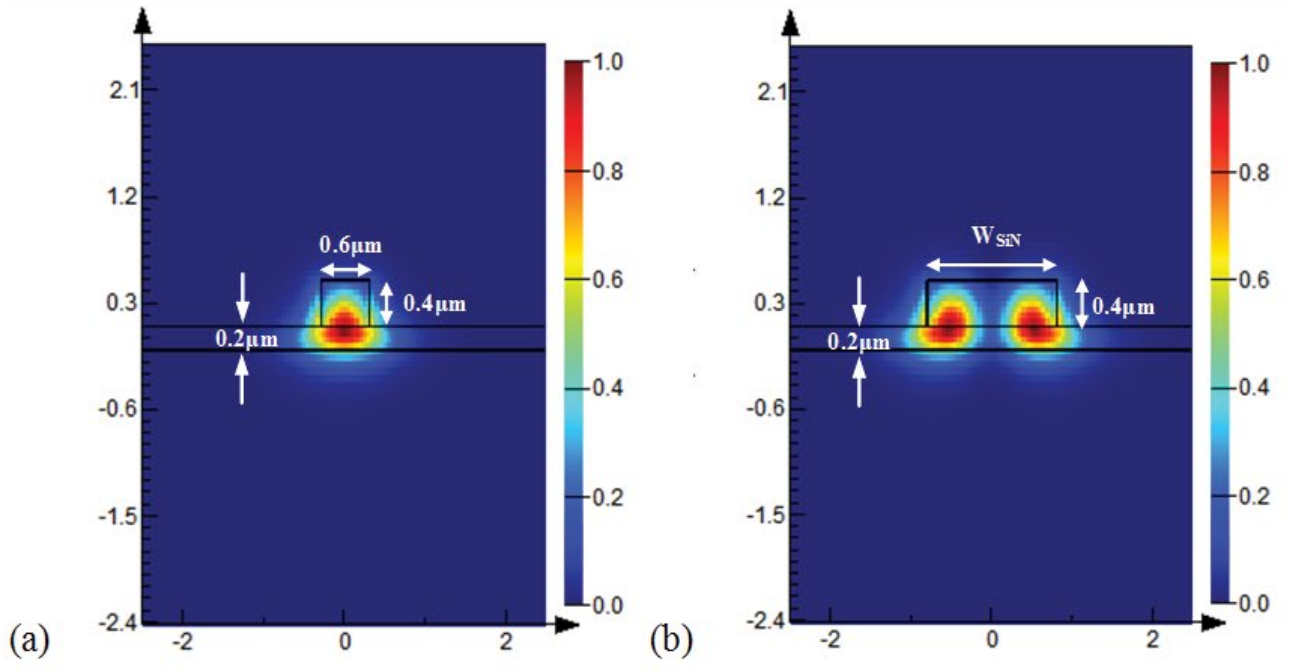

Figure 4: The performance simulation of the ridge waveguide, (a) when it is single-mode transmission, (b) when it is dual-mode transmission.

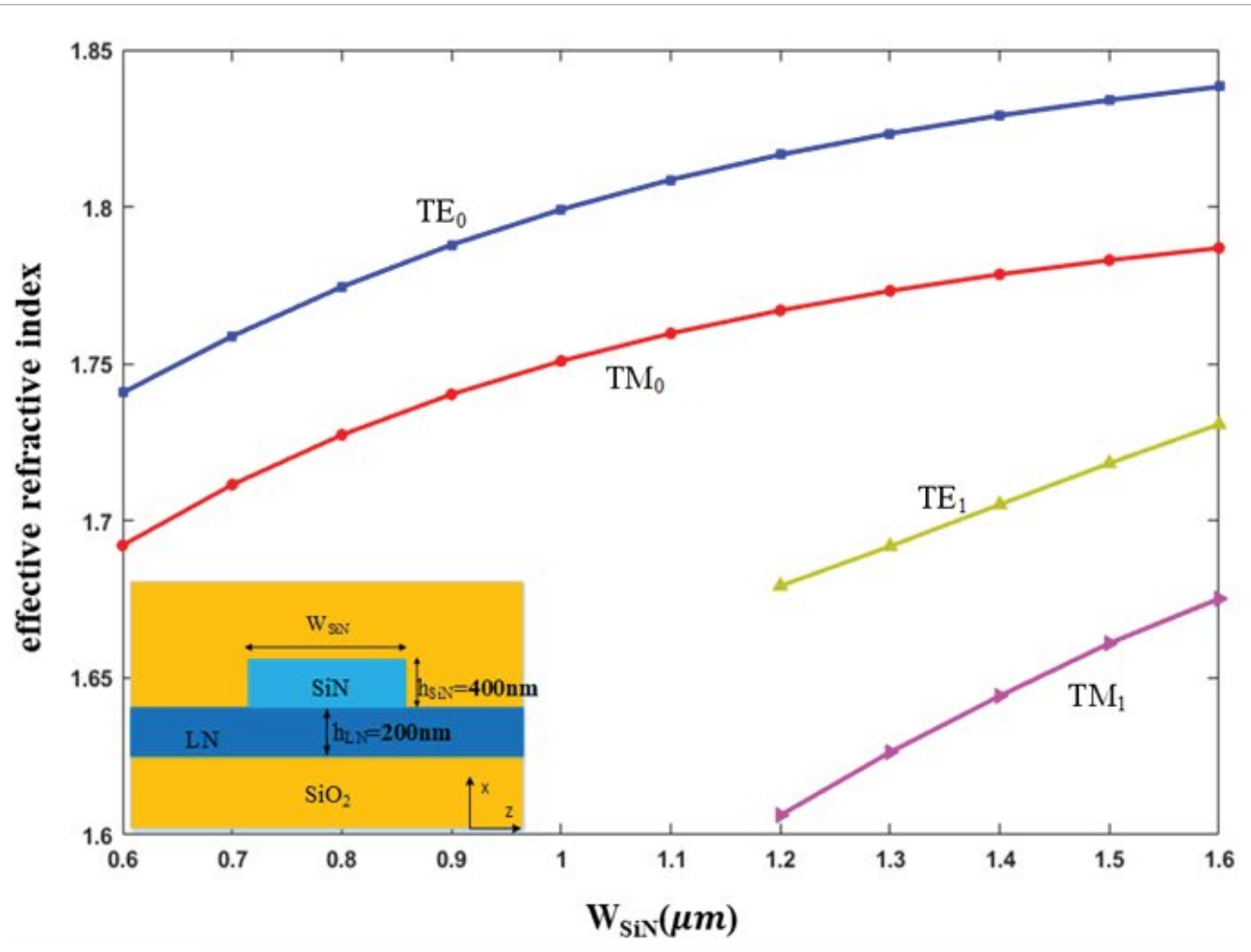

Figure 5: The effective refractive index as the W_{SiN} varies for both TE and TM polarizations.

Citation: Ji W, Liu F, Wu Q, Yin R, (2022) Highly Integrated Polarization Beam Splitter Based on Sin-LNOI Rib Waveguide. Int J Opt Photonic Eng 7:049

to adjust the width of the SiN waveguide so that the ridge waveguide in the multimode interference region satisfies the dual-mode transmission condition. Figure 5 shows that when the thickness of the LN thin film layer is $h_{LN} = 0.2\ \mu m$ and the thickness of the SiN waveguide is $h_{SiN} = 0.4\ \mu m$, the change of the effective refractive index of the ridge waveguide is obtained by adjusting the width of the SiN waveguide W_{SiN}. From the Figure 5, we can find that when the width of the SiN waveguide W_{SiN} varies from 1.2 1.6 μm to 1.6 1.6 μm, the two higher-order modes of TE_1 and TM_1 are excited, which satisfies the dual-mode propagation condition in the ridge waveguide. The effective refractive index difference between TE and TM is about 0.05. The large refractive index difference also ensures that the two polarization states of TE and TM can be separated in a short multimode interference region, thus reducing the overall length of PBS.

After the width range of the ridged waveguide in the multimode interference region is determined, the dual-mode transmission conditions of the waveguide in the multimode interference region are also determined. Then we use the FDTD simulation method to calculate the variation of the nL_C^{TE} and $(n+1)L_C^{TM}$ with W_{SiN}. Figure 6 shows the results of n = 1. Obviously, the growth rate of $2L_C^{TE}$ is greater than that of L_C^{TE}, so when n = 1, the separation of TE and TM polarization cannot be satisfied. By adjusting the width of the SiN waveguide layer W_{SiN} in the LNOI ridge waveguide, we could calculate that the TE and TM polarizations satisfy $L_{CR} = nL_C^{TE} = (n+1)L_C^{TM}$ when n > 1, the required coupling length L_{cr} in the MMI.

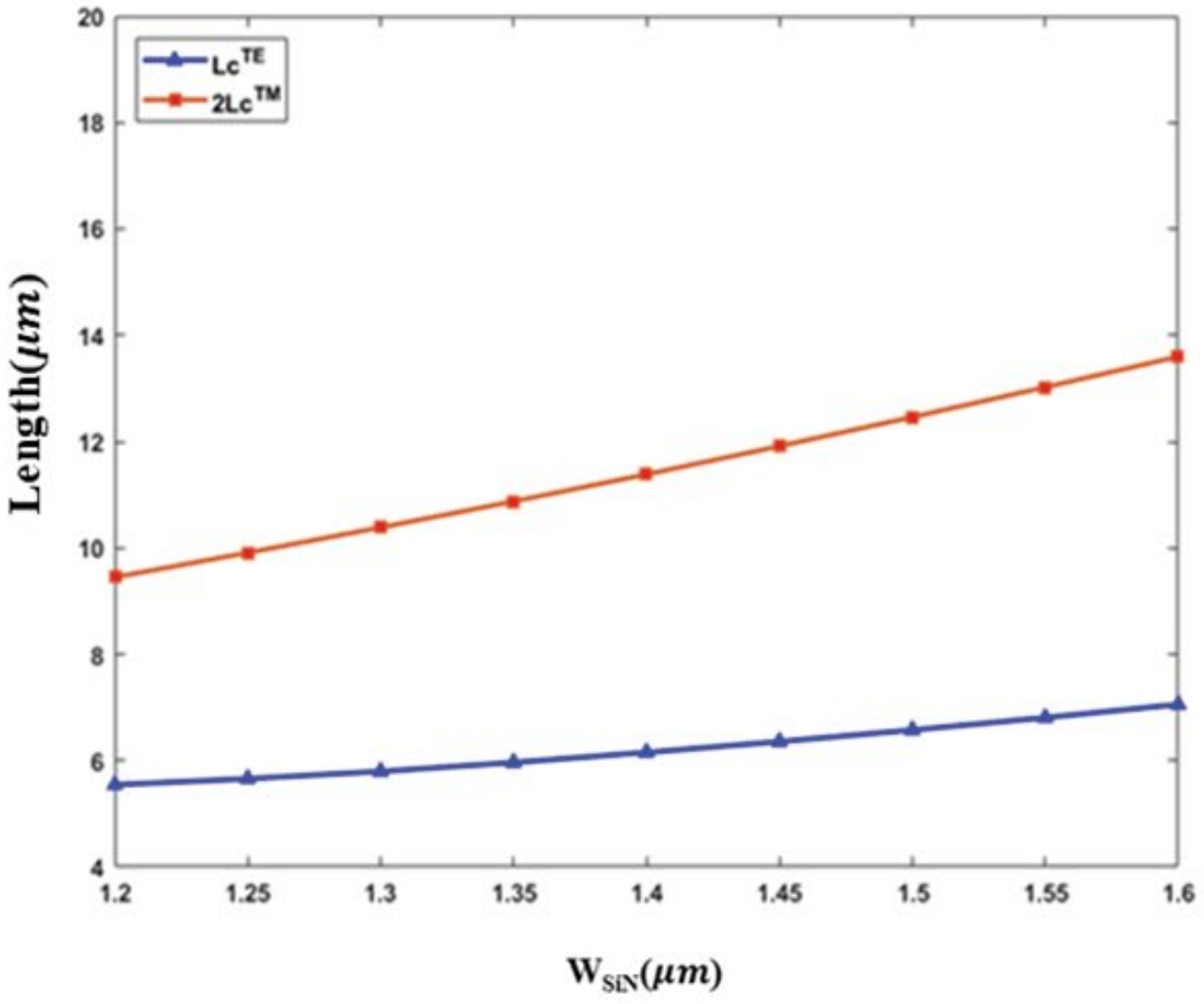

Figure 6: The length of L_C^{TE} and $2L_C^{TE}$ as the width of SiN waveguide varies.

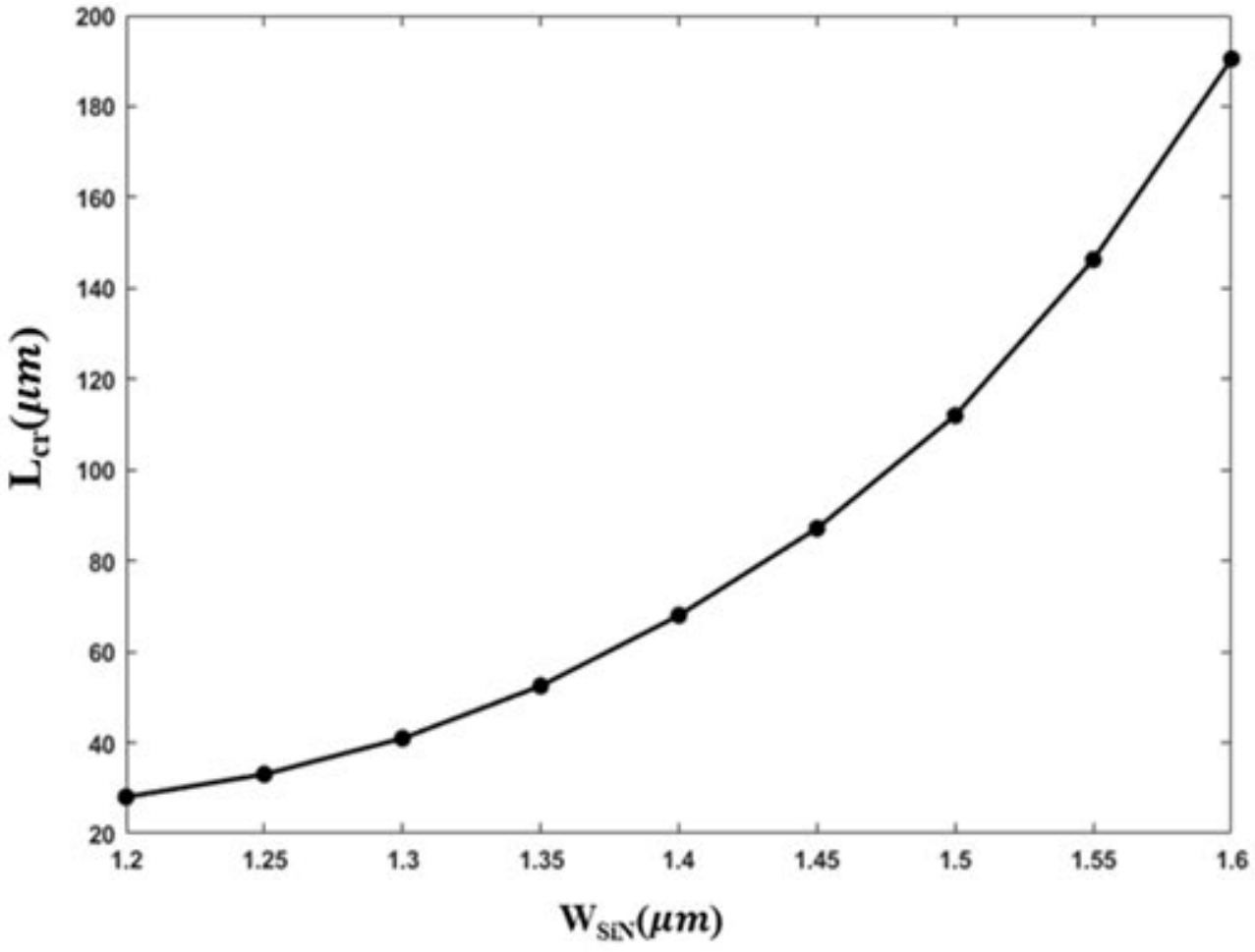

Figure 7: The coupling length L_{cr} of the MMI as the width of SiN waveguide varies.

The results are shown in Figure 7. It is found that with the increase of the W_{SiN}, the coupling length L_{cr} of the MMI is also increased, but the overall length of the coupling region is still less than 200 1.6 μm, compared with the common MMI -based PBS in $LiNbO_3$ [26], the length of the MMI region is about 500 μm. The MMI -based PBS in SiN-$LiNbO_3$ composite ridge waveguide structure has excellent characteristics of small size and high integration.

Simulation and Performance Analysis

For our proposed MMI -based PBS in LNOI, it not only satisfies the needs of small size and high integration, but also needs good polarization separation performance. Similarly, we optimize the width parameters of ridged waveguides in the MMI region by FDTD simulation to ensure the polarization splitting performance, small size and high extinction ratio of PBS. Figure 8 shows the change of extinction ratio of MMI when the width of SiN waveguide varies from 1.2 1.6 μm to 1.6 1.6 μm with the thickness of LN film layer $h_{LN} = 0.2$ μm and SiN waveguide layer $h_{SiN} = 0.4$ μm. When the central wavelength of PBS is λ = 1550 nm , the extinction ratio of TE and TM polarizations in the MMI increases with the increase of ridge width W_{SiN}. According to the simulation results in Figure 5, the MMI cannot satisfy the dual-mode transmission condition when the waveguide ridge width is greater than 1.6 μm. Therefore, when the W_{SiN} is 1.6 μm, the extinction ratio of TE and TM polarizations in the MMI is the highest. The extinction ratio of TE mode and TM mode is 16.79 dB and 25.74 dB respectively.

Since the extinction ratio range of PBS is higher than 10dB, it can be seen from Figure 8 that in the MMI region, the width process tolerance of ridge waveguides in TE mode is 200 nm and the width process tolerance of ridge waveguides in TM mode is larger than 300 nm. In order to ensure

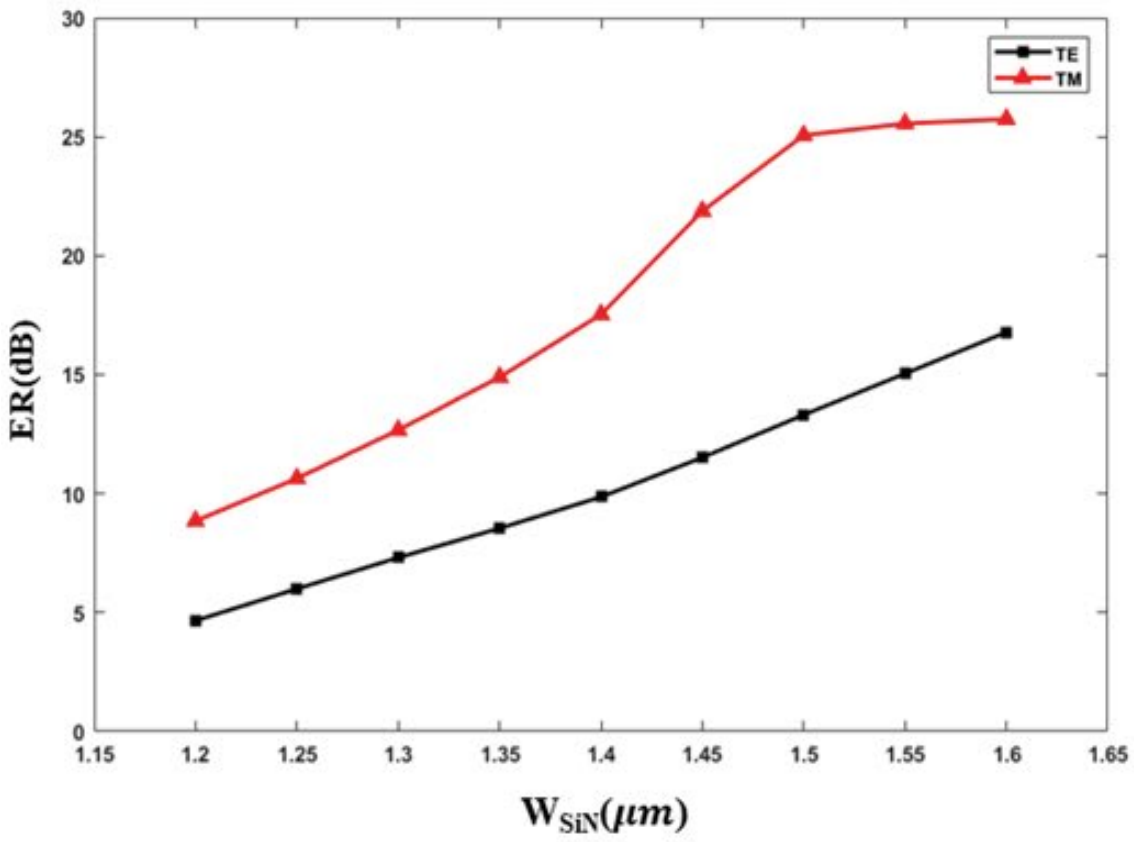

Figure 8: The extinction ratio as the width of SiN waveguide varies.

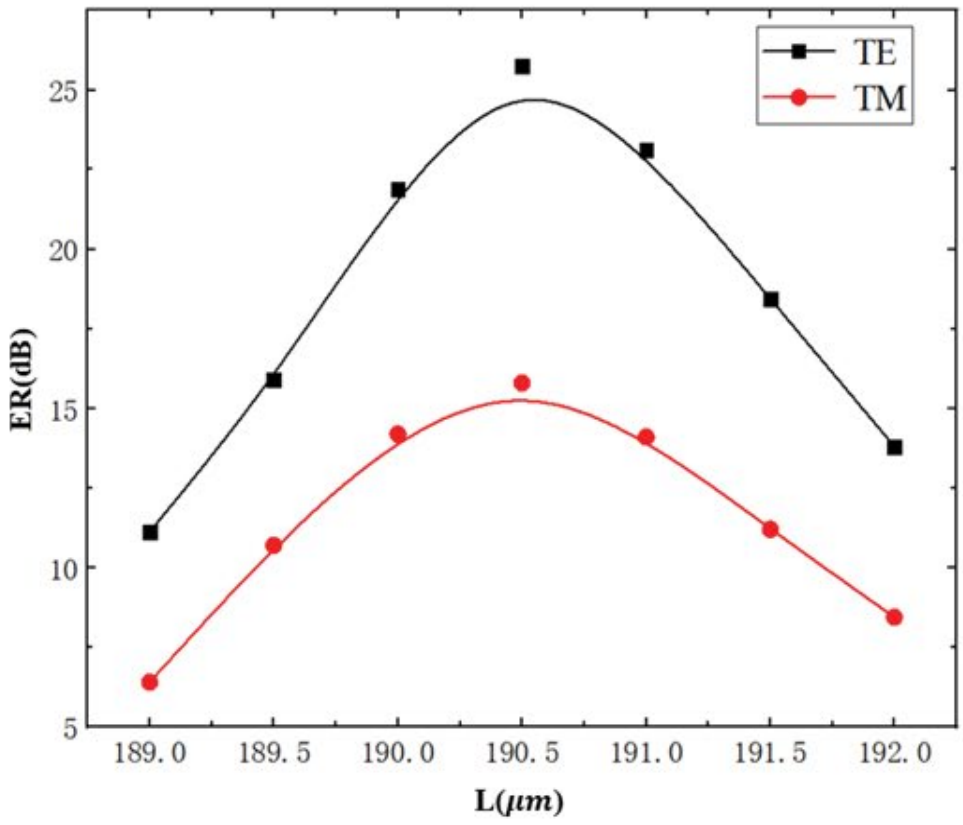

Figure 9: The extinction ratio as the length of MMI waveguide L varies.

the highest extinction ratio, we set the structure parameters of the waveguide in the MMI as follows: $h_{LN} = 0.2\ \mu m$, $h_{SiN} = 0.4\ \mu m$ and $W_{SiN} = 1.6\ \mu m$. At the same time, in order to make the extinction ratio of TE and TM more close, we further optimize the extinction ratio of PBS by adjusting the length of the MMI. Figure 9 shows the variation of the extinction ratio of TE and TM polarizations when the length of the MMI ranges from 189 μm to 192 μm. With the increase of MMI length L, the ER of both TE and TM polarizations increases at first and then decreases. According to the FDTD simulation results, for the maximum extinction ratio of TE and TM polarizations, the coupler length L is 190.5 μm, but considering the optimization of the extinction ratio difference between TE and TM polarizations, we finally take the length L of the MMI as 190.3 μm (Table 1).

Figure 9 shows that in the multimode interference region of PBS, when the dual-mode transmission conditions of ridge waveguides are satisfied, the different performance parameters of MMIs are obtained by taking different values of the LN film thickness. By comparison, it is found that when the LN film thickness increases, although the coupling distance L_{cr} of the MMI decreases and the device process tolerance increases slightly, the extinction ratio of the device decreases obviously, so to sum up, we still define the thickness of the LN thin film h_{LN} as 0.2 μm. In this section, we simulate the light propagation of TE and TM in the MMI at λ = 1550 nm by using 3D-FDTD. The light field simulation is shown in Figure 10a and Figure 10b, respectively. It can be seen that the launched TE polarization is coupled odd times and output from the cross port, while the TM polarization is coupled even times and output from the through port, which realizes the separation of TE and TM polarizations. Moreover, the extinction ratio of TE and TM polarizations is greater than 15dB.

Conclusion

In this paper, we propose a multimode

Table 1: Different values of LN film thickness performances.

LN film thickness (μm)	Lcr (μm)	ER (dB)		fabrication tolerances (nm)
		TE	TM	
0.2	190.3	16.7	24.3	200
0.3	47.2	12.8	20.2	200
0.4	36.84	9.4	16.7	300

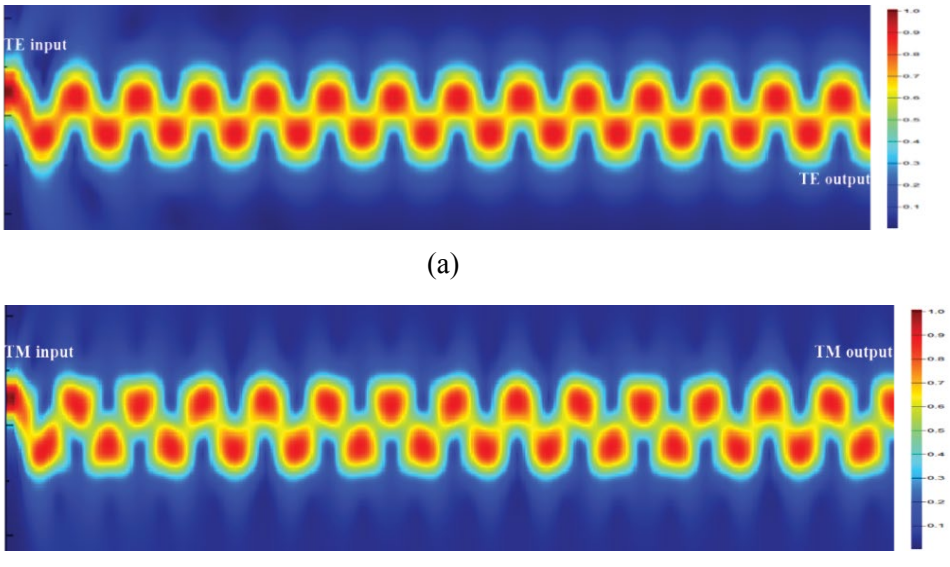

Figure 10: The performance simulation of the proposed PBS, (a) when TE mode is launched, (b) when TM mode is launched.

interference (MMI)-based PBS in X-cut LNOI. The device is designed and simulated by using three dimensional finite difference time domain (3D-FDTD) method. The width of the ridge waveguide, the thickness of the LN film and the length of the coupler in the multimode interference region are optimized to obtain the optimal coupling length, extinction ratio and manufacturing tolerance. The device is simple in structure and easy to implement. At the same time, the LNOI platform is used to design the hybrid integration of LN thin film and SiN thin film which is easy to be etched, the MMI length of PBS is 190.3 μm, the extinction ratio is above 15dB, and the device fabrication tolerance is larger than 200 nm.

Acknowledgements

This study is supported by The National Key Research and Development Program of China (2018YFC0831103), National natural science foundation (61571273), Natural Science Foundation of Shandong Province (ZR2021MF018), Open Fund of IPOC 2021 (BUPT) and the Research Funds of Hisense Broadband

References

1. Lin J, Bo F, Cheng Y, Xu Y (2020) Advances in on-chip photonic devices based on lithium niobate on insulator. Photonics Research 8: 1910-1936.
2. Li GL, Jia YC, Chen F (2020) Research progress of photonics devices on lithium-niobate-on-insulator thin films. Acta Phys Sin -Chinese Edition 69: 157801.
3. Krasnokutska I, Tambasco JLJ, Peruzzo A (2019) Tunable large free spectral range microring resonators in lithium niobate on insulator[J]. Scientific Reports 9: 11086.
4. Ying L, Lan T, Li J, Wang Z (2020) Study on high efficiency edge-coupling based on lithium niobate on insulator wire waveguide. Appl Opt 59: 6694-6701.
5. Bhandari B, Im C, Sapkota OR, Lee SS (2020) Highly efficient broadband silicon nitride polarization beam splitter incorporating serially cascaded asymmetric directional couplers. Opt Lett 45: 5974-5977.
6. Bai B, Pei L, Zheng J, Ning T, Li J (2020) Ultra-short plasmonic polarization beam splitter-rotator using a bent directional coupler. Chinese Optics Letters 18: 041301.
7. Chen Y, Xiao J (2020) Compact silicon-based polarization beam splitter using directional couplers assisted with subwavelength gratings. Optical Engineering 59: 017101.
8. Wang D, Hu Y, Yue W, Zheng Y, Tu Z, et al. (2019) Broadband and compact polarization beam splitter based on an asymmetrical directional coupler with extra optimizing designs. Appl Opt 58: 8221-8226.
9. Zhao N, Qiu C, He Y, Zhang Y, Su Y (2019) Broadband polarization beam splitter by using cascaded tapered bent directional couplers. Photonics Journal IEEE 11: 1-8.
10. Huang T, Xie Y, Wu Y, Cheng Z, Seng S, et al. (2019) Compact polarization beam splitter assisted by subwavelength grating in triple-waveguide directional coupler. Appl Opt 58: 2264-2268.
11. Kim Y, Lee MH, Kim Y, Kim KH (2018) High-extinction-ratio directional-coupler-type polarization beam splitter with a bridged silicon wire waveguide. Opt Lett 43: 3241-3244.
12. Chang lM, Liu L, Gong YH, Tan MQ, Yu YD, et al. (2018) Polarization-independent directional coupler and polarization beam splitter based on asymmetric cross-slot waveguides. Appl Opt 57: 678-683.
13. Xu H, Dai D, Liu L, Shi Y (2020) Proposal for an ultra-broadband polarization beam splitter using anisotropy-engineered Mach-Zehnder interferometer on x-cut lithium-niobate-on-insulator. Opt Express 28: 10899-10908.
14. Koshelev AY, Gol'tsov AY (2013) Fabrication-tolerant integrated polarisation splitter based on cascaded Mach-Zehnder interferometers. Quantum Electron 43: 1154-1158.
15. Dai D, Wang Z, Peters J, Bowers JE (2012) Compact polarization beam splitter using an asymmetrical Mach-Zehnder interferometer based on silicon-on-insulator waveguides. IEEE Photonics Technol Lett 24: 673-675.
16. Farhadi S, Miri M, Alighanbari A (2020) Design and simulation of a compact and ultra-wideband polarization beam splitter based on sub-wavelength grating multimode interference coupler. Applied Physics B 126: 1-11.
17. Hassan S, Chack D, Mahajan V (2020) High extinction ratio and low loss polarization beam splitter based on multimode interference for PICs. Appl Opt 59: 3369-3375.
18. Yin M, Yang W, Li Y, Wang X, Li H (2015) CMOS-compatible and fabrication-tolerant MMI-based polarization beam splitter. Opt Commun 335: 48-52.
19. Qu Y, Yuan J, Zhou X, Li F, Yan B, et al. (2020) Surface plasmon resonance-based silicon dual-core

photonic crystal fiber polarization beam splitter at mid-infrared spectral region. Journal of the Optical Society of America B 37: 2221-2230.

20. Chen N, Zhang X, Lu X, Zhang Z, Mu Z, et al. (2020) Numerical investigation of a short polarization beam splitter based on dual-core photonic crystal fiber with As2S3 layer. Micromachines (Basel) 11: 706.

21. Mishra V, Varshney R, Kumar S (2020) Design of a compact and broadband THz polarization splitter based on gradient dual core photonic crystal fiber. Appl Opt 59: 1974-1979.

22. Rao A, Fathpour S (2018) Heterogeneous thin-film lithium niobate integrated photonics for electrooptics and nonlinear optics. IEEE Journal of Selected Topics in Quantum Electronics 99: 1-1.

23. Amirmahdi H, Camacho G, Saeed K, Malinowski M, Rao A, et al. (2018) Cascaded integration of optical waveguides with third-order nonlinearity with lithium niobate waveguides on silicon substrates. IEEE Photonics Journal 10: 1-9.

24. Fathpour S, Rao A, Rabiei P, Patil A, DeSalvo R, et al. (2016) Heterogeneous lithium niobate microring and modulator integration on silicon (Invited). IEEE International Topical Meeting on Microwave Photonics, IEEE, Long Beach, CA, USA.

25. Darmawan S, Lee SY, Lee CW, Chin MK (2005) A rigorous comparative analysis of directional couplers and multimode interferometers based on ridge waveguides. IEEE J Sel Top Quantum Electron 11: 466-475.

26. Sharapova P, Luo KH, Herrmann H, Reichelt M, Meier T, et al. (2017) Generation and active manipulation of qubits in $LiNbO_3$-based integrated circuits.

DOI: 10.35840/2631-5092/4549